

# Critical dynamics of Model H within the real-time fRG approach

Yong-rui Chen,<sup>1</sup> Yang-yang Tan,<sup>1</sup> and Wei-jie Fu<sup>1</sup>

<sup>1</sup>*School of Physics, Dalian University of Technology, Dalian, 116024, P.R. China*

The critical dynamics of Model H with a conserved order parameter coupled to a transverse momentum density which describes the gas-liquid or binary-fluid transitions is investigated within the functional renormalization group approach formulated on the closed time path. According to the dynamic scaling analysis, Model H and QCD critical end point belong to the same dynamic universality class in the critical region. The higher-order correction of the transport coefficient  $\bar{\lambda}$  and shear viscosity  $\bar{\eta}$  arising from mode-couplings are obtained by calculating the two-point correlation functions. The flow equation of a dimensionless coupling constant for nondissipative interactions is derived to look for the fixed-point solution of the system. The scaling relation between the critical exponent of the transport coefficient and that of the shear viscosity is estimated. Finally, the dynamic critical exponent  $z$  is obtained as a function of the spatial dimension  $d$ .

## I. INTRODUCTION

Critical dynamics plays a crucial role in the studies of QCD phase structure that is related to the phase transition from the confinement hadronic phase to the deconfinement phase of quark-gluon plasma (QGP) [1–4]. It is expected that fluctuations of conserved charges can be used to search for the critical end point (CEP) in heavy-ion collision experiments [5–9]. Significant progresses have been made in the Beam Energy Scan (BES) program at Relativistic Heavy Ion Collider (RHIC) [10–13]. Notably, recent estimates of the location of CEP in the QCD phase diagram have arrived at convergent results from functional QCD [14–16], which are also consistent with the results obtained from finite-size scaling of proton cumulants in heavy-ion collisions [17] and from extrapolation of lattice simulations [18]. The correlation length tends to be divergent near the CEP, such that properties of the critical behavior are universal and independent of the detail of microscopic interactions. It is found that the chiral phase transition at vanishing chemical potential in the chiral limit of  $u$  and  $d$  quarks is classified into the universality of three dimensional ( $3d$ )  $O(4)$  symmetry [19], and the CEP in the QCD phase diagram belongs to the  $Z(2)$  universality class [20], see also e.g., [21] for relevant discussions.

The criticality is not only reflected in static equilibrium properties, but also in real-time nonequilibrium dynamics. When the critical end point is approached, the relaxation time from nonequilibrium to equilibrium is significantly increased, that is known as the effect of critical slowing down [22, 23]. The renormalization group technique by Wilson *et al.* have been extended to study the dynamic critical phenomena [24–27], where several characteristic dynamic universalities were investigated and classified, see [28, 29] for related reviews. It has been shown that the second-order chiral phase transition of QCD lies in the dynamic universality class of ‘Model G’ [22], and the dynamics of QCD critical end point belongs to ‘Model H’ [30]. A plethora of results about the real-time correlation functions and critical dynamics have been obtained within the classical-statistical lattice

simulations [31–36]. Recently, the functional renormalization group (fRG) within the Schwinger-Keldysh formalism [37–41] has been used to investigate the spectral functions [42–44], pseudo-Goldstone damping [45], critical dynamics and dynamic critical exponents in Model A [46–50], Model C [46, 51] and Model G [52] and so forth. This provides us with a powerful tool to explore the critical dynamics of fluctuations with nonperturbative interactions.

In this work we would like to study the properties of dynamic universality class ‘Model H’ using the real-time fRG approach. Model H is characterized by a conserved order parameter field, which can be treated as a combination of the chiral condensate and baryon density in QCD, and this order parameter couples with the energy-momentum density. That is related to the liquid-gas phase transition. Previous studies focus on the perturbative  $\epsilon$ -expansion method, see [53, 54]. Recently stochastic fluid dynamics simulation has also been performed on Model H [55]. From the equation of motion, we construct the effective action in terms of two different kinds of field with the Keldysh rotation [56, 57]. The mode-couplings and dissipative dynamics are encoded through the calculations of correlation functions. By solving the fixed-point equations we obtain the anomalous dimensions and dynamic critical exponent.

This paper is organized as follows: In Sec. II we briefly introduce the Langevin equation of Model H. The formalism of Model H formulated on the closed time path within the fRG approach is specialized in Sec. III, where the flow equations of the effective potential and relevant parameters are shown. Numerical results are presented and discussed in Sec. IV. In Sec. V we give a summary and conclusion. The expressions of the propagators and Feynman rules of vertices are collected in App. A. In App. B, we show a specific calculation for loop diagram.

## II. LANGEVIN EQUATION FOR MODEL H

The simplified model that describes the dynamics of the gas-liquid or binary-fluid transition was introduced

earlier in the mode-coupling theories, which was denoted as Model H [28, 53]. The equations of motion for the coupled modes in Model H are given by the Langevin equations

$$\frac{\partial \phi}{\partial t} = \lambda_0 \nabla^2 \frac{\delta \mathcal{H}}{\delta \phi} - g_0 \nabla \phi \cdot \frac{\delta \mathcal{H}}{\delta \mathbf{j}} + \theta(x, t), \quad (1)$$

$$\frac{\partial \mathbf{j}}{\partial t} = \Pi^\perp \left( \eta_0 \nabla^2 \frac{\delta \mathcal{H}}{\delta \mathbf{j}} + g_0 \nabla \phi \frac{\delta \mathcal{H}}{\delta \phi} + \zeta(x, t) \right), \quad (2)$$

with the Hamiltonian

$$\mathcal{H} = \int d^d x \left( \frac{1}{2} |\nabla \phi(x)|^2 + \frac{r}{2} \phi^2 + \frac{u}{4} \phi^4 + \frac{1}{2} \mathbf{j}^2 \right). \quad (3)$$

The correlations of Gaussian noises read

$$\begin{aligned} \langle \theta(x, t) \theta(x', t') \rangle &= -2\lambda_0 \nabla^2 \delta(x - x') \delta(t - t'), \\ \langle \zeta_\mu(x, t) \zeta_\nu(x', t') \rangle &= -2\eta_0 \nabla^2 \delta(x - x') \delta(t - t') \delta_{\mu\nu}. \end{aligned} \quad (4)$$

The scalar field  $\phi$  of order parameter is a conserved quantity. The vector field  $\mathbf{j}$  corresponds to the momentum density or velocity, that has only the transverse components, since the right hand side of equation of motion for  $\mathbf{j}$  in Eq. (2) is multiplied by the transverse projection operator, i.e.,

$$\Pi_{\alpha\beta}^\perp = (\delta_{\alpha\beta} - \mathbf{q}_\alpha \mathbf{q}_\beta / \mathbf{q}^2). \quad (5)$$

In Eq. (1) and (2)  $\lambda_0$  and  $\eta_0$  are the transport coefficient and shear viscosity, respectively. Their dynamical scaling behaviors are described by the exponents  $x_\lambda$  and  $x_\eta$  in the critical regime, and these exponents can also be seen as dynamic anomalous dimensions. The Hamiltonian has the usual form except the term  $\mathbf{j}^2/2$  included. Thus the static critical properties of  $\phi$  are the same as the Ginzburg-Landau model with Ising symmetry. When the system is in thermal equilibrium, the equilibrium distribution function is given by  $e^{-\mathcal{H}}$ . The coupling constant  $g_0$  describes the interaction between the two dynamical modes in model H. The Gaussian noises  $\theta$  and  $\zeta$  derive the system to thermal equilibrium and their correlation functions are shown in Eq. (4).

According to the dynamic scaling relation, the characteristic frequency of the order parameter has the following form [58]

$$\omega_\phi(k) = Dk^2 \Omega(k\xi) = D_0 \xi^{2-z} k^2 \Omega(k\xi), \quad (6)$$

in the limit  $\xi \rightarrow \infty, k \rightarrow 0$ . Here  $\xi$  is the correlation length, and the diffusion constant  $D$  satisfies the ‘Kawasaki-Stokes’ relation [59, 60]

$$D = \frac{\lambda}{\chi_\phi} = \frac{Rk_B T}{\eta \xi}, \quad (7)$$

with the static susceptibility  $\chi_\phi$ . Consequently, one arrives at the dynamic critical exponent  $z$  for the order parameter

$$z = 4 - \eta_\phi - x_\lambda, \quad (8)$$

where  $\eta_\phi$  is the static anomalous dimension. The results of the exponents  $x_\lambda$  and  $x_\eta$  in the  $\epsilon$ -expansion up to the order of  $O(\epsilon^2)$  are obtained as [53]

$$\begin{aligned} x_\lambda &= \frac{18}{19} \epsilon [1 - 0.033\epsilon + O(\epsilon^2)], \\ x_\eta &= \frac{1}{19} \epsilon [1 + 0.238\epsilon + O(\epsilon^2)]. \end{aligned} \quad (9)$$

In the next section, we will compute the above exponents using the functional renormalization group approach.

### III. MODEL H WITHIN THE REAL-TIME FRG APPROACH

The crucial part of the functional renormalization group (fRG) approach is the scale-dependent effective action  $\Gamma_k[\Phi]$  that interpolates smoothly between the short-distance and long-distance physics with the evolution of the exact renormalization group equation [61], for fRG reviews see [2, 3, 62]. At the ultraviolet cutoff  $k = \Lambda$ , the effective action  $\Gamma_\Lambda[\Phi]$  coincides with the classical action  $S[\Phi]$  and at  $k = 0$  the effective action is the quantum action as fluctuations of different momentum modes are integrated in successively. To formulate the effective action in the closed time path, starting from the Langevin equation in Eq. (1) and (2), we perform the path integral about the noise variables that result in the Martin-Siggia-Rose response field [63]. The renormalization group (RG) scale  $k$  dependent effective action of Model H in the Schwinger-Keldysh formalism is

$$\begin{aligned} \Gamma_k[\Phi] &= i \int d^d x dt \phi_q \left( \frac{\partial}{\partial t} \phi_c + \lambda_k \nabla^2 \nabla^2 \phi_c \right) \\ &\quad - \lambda_k \phi_q \nabla^2 \frac{\delta V_k(\rho_c)}{\delta \phi_c} + g_k \phi_q \nabla \phi_c \cdot \mathbf{j}_c + 2\lambda_k \phi_q \nabla^2 \phi_q \\ &\quad + \mathbf{j}_{q,\alpha} \Pi_{\alpha\beta}^\perp \left[ \left( \frac{\partial}{\partial t} \mathbf{j}_{c,\beta} - \eta_k \nabla^2 \mathbf{j}_{c,\beta} \right) \right. \\ &\quad \left. - g_k \nabla \phi_c (-\nabla^2 \phi_c) + 2\eta_k \nabla^2 \mathbf{j}_{q,\beta} \right]. \end{aligned} \quad (10)$$

Here,  $(\phi_c, \phi_q)$  and  $(\mathbf{j}_{c,\beta}, \mathbf{j}_{q,\alpha})$  are the order parameter fields and momentum densities with the subscripts ‘c’ and ‘q’ denoting classical and quantum fields, respectively, see [43, 47] for more details. And subscripts  $\alpha, \beta$  denote the component of vector  $\mathbf{j}$ , i.e.,  $\alpha, \beta = 1, 2, \dots, d$ . Different from the analogue in Eq. (1) and (2), the transport and coupling constants  $\lambda_k, \eta_k$  and  $g_k$  in Eq. (10) also receive corrections from interactions, and they are RG-scale dependent. Note that the order parameter belongs to the Ising universality class, thus presents the same static critical properties. The order parameter can be regarded as a linear combination of the chiral condensate and baryon density in QCD [30]. Moreover, one can see that the powers of gradient in front of  $\phi_c$  are higher than those in Model A or Model C due to the conservation of the order

parameter and momentum. The higher order scatterings among the  $\phi$  fields are encoded in the effective potential as well as the mass term of order parameter.

$$iG_{\phi,k}^R = \text{---} \underset{c}{\text{---}} \underset{q}{\text{---}}, \quad iG_{\phi,k}^A = \text{---} \underset{q}{\text{---}} \underset{c}{\text{---}}, \quad iG_{\phi,k}^K = \text{---} \underset{c}{\text{---}} \underset{c}{\text{---}}$$

$$iG_{j,k}^R = \text{---} \underset{c}{\text{---}} \underset{q}{\text{---}}, \quad iG_{j,k}^A = \text{---} \underset{q}{\text{---}} \underset{c}{\text{---}}, \quad iG_{j,k}^K = \text{---} \underset{c}{\text{---}} \underset{c}{\text{---}}$$

FIG. 1: Diagrammatic representation of the retarded, advanced and Keldysh propagators for the order parameter and momentum density fields in this work.

The flow equation of the effective action reads

$$\partial_\tau \Gamma_k[\Phi] = \int G_k \partial_\tau R_k, \quad (11)$$

with the propagator  $G_k$

$$G_k = \frac{1}{\Gamma_k^{(2)}[\Phi] + R_k}, \quad (12)$$

where  $R_k$  stands for the regulator and  $\Gamma_k^{(2)}[\Phi]$  the second derivative of  $\Gamma_k$  with respect to the fields. In this context, the related fields are the order parameter and transverse momentum density. We present the expression of the propagators and three-point coupling vertices in App. A. To be simplified, we directly show the matrix form of the propagator that is

$$G_k = \begin{pmatrix} G_k^K & G_k^R \\ G_k^A & 0 \end{pmatrix}, \quad (13)$$

where  $K, R$  and  $A$  denote the Keldysh, retarded and advanced propagators, respectively. In Fig. 1 we show the diagrammatic representation for the relevant propagators, the dashed lines denote the order parameter and the wave lines denote the vector momentum density.

In the following, we will apply the real-time fRG approach to compute the flow equations of effective potential  $V_k(\rho)$ , transport coefficient  $\lambda_k$  and shear viscosity  $\eta_k$  and coupling constant  $g_k$ . The flow of effective potential corresponds to the one-point correlation function of  $\Gamma_k[\Phi]$  with respect to the field  $\phi_q$  as shown in Fig. 2,

$$\partial_\tau V'_k(\rho) = \int_{\omega,q} \frac{1}{2} \Gamma_{\phi_q \phi_c \phi_c, k}^{(3)} \tilde{\partial}_\tau G_{\phi \phi, k}^K / (-\lambda_k \nabla^2), \quad (14)$$

with the explicit form of vertex  $\Gamma_{\phi_q \phi_c \phi_c, k}^{(3)}$  shown in App. A. The flow equation of  $V'_k(\rho)$  is the same as Model A with one component of the order parameter.

The flow for the  $\lambda_k$  and  $\eta_k$  are related to the inverse of retarded propagators for the order parameter and momentum density fields respectively, which can be

$$\partial_\tau \left( \text{---} \underset{q}{\text{---}} \underset{c}{\text{---}} \right) = \frac{1}{2} \tilde{\partial}_\tau \left( \text{---} \underset{q}{\text{---}} \underset{c}{\text{---}} \right)$$

FIG. 2: Diagrammatic representation of the flow equation for the effective potential obtained from the one-point correlation function of the effective action actually. The external leg denotes the field  $\phi_q$  and the internal line denotes the Keldysh type propagator for the order parameter.

$$\partial_\tau \left( \text{---} \underset{q}{\text{---}} \underset{c}{\text{---}} \right) = \tilde{\partial}_\tau \left( \text{---} \underset{q}{\text{---}} \underset{c}{\text{---}} \right) + \text{---} \underset{q}{\text{---}} \underset{c}{\text{---}} \text{---}$$

$$\partial_\tau \left( \text{---} \underset{q}{\text{---}} \underset{c}{\text{---}} \right) = \tilde{\partial}_\tau \left( \text{---} \underset{q}{\text{---}} \underset{c}{\text{---}} \right)$$

FIG. 3: Diagrammatic representation of the flow equation for the inverse retarded propagator related to the order parameter and momentum density fields, see Eq. (15).

obtained by projecting onto the external momentum direction, to wit,

$$\partial_\tau \lambda_k = \lim_{\substack{p_0 \rightarrow 0 \\ \mathbf{p} \rightarrow 0}} (-i) \frac{\partial}{\partial \mathbf{p}^4} \frac{\delta^2 \partial_\tau \Gamma_k[\Phi]}{\delta \phi_q(-p) \delta \phi_c(p)} \Big|_{\Phi_{\text{EoM}}},$$

$$\partial_\tau \eta_k = \frac{1}{d-1} \lim_{\substack{p_0 \rightarrow 0 \\ \mathbf{p} \rightarrow 0}} (-i) \frac{\partial}{\partial \mathbf{p}^2} \frac{\delta^2 \partial_\tau \Gamma_k[\Phi]}{\delta \mathbf{j}_{q,\alpha}(-p) \delta \mathbf{j}_{c,\beta}(p)} \Pi_{\alpha\beta}^\perp \Big|_{\Phi_{\text{EoM}}}, \quad (15)$$

with the factor  $1/(d-1)$  in the flow of  $\eta_k$  arising from the transverse projection operator. We show the diagrammatic representation for the two-point correlation function of the corresponding fields in Fig. 3. Here the partial operator  $\tilde{\partial}_\tau$  hits the  $k$ -dependence only through the regulator in propagators. This provides us with all the possible diagrams we need to calculate. And the types of propagators and vertices are labelled in the diagrams with the letters ‘q’ and ‘c’. Since the external momentum information is contained in the vertices and propagators, the final result on the power of external momenta should account for the contributions from both the vertices and propagators.

Here we also introduce the dimensionless quantities to convert the flow equations to fixed-point equations which is more convenient to investigate the scaling behavior,

such as

$$\begin{cases} \bar{\lambda} = k^{4-z}\lambda_k \\ \bar{\eta} = k^{2-z}\eta_k \\ \bar{g} = k^{1+\frac{d}{2}-z}g_k \\ \bar{\rho} = k^{2-d}\rho \\ u(\bar{\rho}) = k^{-d}V_k(\rho) \end{cases}. \quad (16)$$

In App. B, a specific example for the loop diagram calculation is presented for illustrative purpose, where we also show the expansion up to certain power of external momentum and the related approximation used there. Performing the integrals on the right hand side of Fig. 2 and Fig. 3, one arrives at the final form of the flow equations for the effective potential  $u'(\bar{\rho})$ , and the coefficients  $\bar{\lambda}$ ,  $\bar{\eta}$ ,  $\bar{g}$  as follows

$$\begin{aligned} \partial_\tau u'(\bar{\rho}) = & (-2 + \eta_\phi)u'(\bar{\rho}) + (-2 + d + \eta_\phi)\bar{\rho}u^{(2)}(\bar{\rho}) \\ & - \frac{2\nu_d}{d} \left(1 - \frac{\eta_\phi}{d+2}\right) \left(\frac{3u^{(2)}(\bar{\rho}) + 2\bar{\rho}u^{(3)}(\bar{\rho})}{(1 + u'(\bar{\rho}) + 2\bar{\rho}u^{(2)}(\bar{\rho}))^2}\right), \end{aligned} \quad (17)$$

$$\begin{aligned} \partial_\tau \bar{\lambda} = & -(z - 4 + \eta_\phi)\bar{\lambda} \\ & - \frac{2\bar{g}^2}{\bar{\eta}} \frac{1}{(1 + \bar{m}^2)^2} \int d\Omega_d (-1 + \cos^2 \theta) \cos^2 \theta \\ & + \frac{2}{d} \frac{2\bar{g}^2}{\bar{\eta}} \frac{1}{(1 + \bar{m}^2)^2} \int d\Omega_d (2 - 6\cos^2 \theta + 4\cos^4 \theta) \\ & - \frac{2\bar{g}^2}{\bar{\eta}} \frac{1}{1 + \bar{m}^2} \int d\Omega_d (\cos^4 \theta - \cos^2 \theta) \\ & + \frac{6\bar{g}^2\bar{\lambda}}{\bar{\eta}^2} \int d\Omega_d (-1 + \cos^2 \theta) \cos^2 \theta \\ & + \frac{2}{d+2} \frac{6\bar{g}^2\bar{\lambda}}{\bar{\eta}^2} (1 + \bar{m}^2) \int d\Omega_d (-1 + \cos^2 \theta) \\ & - \frac{3\bar{g}^2\bar{\lambda}}{\bar{\eta}^3} \int d\Omega_d (4\cos^2 \theta - 4\cos^4 \theta) \\ & + \frac{2}{d+4} \frac{32\bar{g}^2\bar{\lambda}^2}{\bar{\eta}^3} (1 + \bar{m}^2) \int d\Omega_d (\cos^2 \theta - \cos^4 \theta), \end{aligned} \quad (18)$$

$$\begin{aligned} \partial_\tau \bar{\eta} = & -(z - 2)\bar{\eta} \\ & + \frac{2}{d} \frac{\bar{g}^2}{\bar{\lambda}} \frac{1}{(1 + \bar{m}^2)^3} \int d\Omega_d (1 - 3\cos^2 \theta + 2\cos^4 \theta), \end{aligned} \quad (19)$$

$$\partial_\tau \bar{g} = -(z - 3 + (4 - d)/2)\bar{g}, \quad (20)$$

where  $d\Omega_d$  represents the angular integration in  $d$ -dimension. The renormalized dimensionless mass square of the order parameter reads

$$\bar{m}^2 = u'(\bar{\rho}) + 2\bar{\rho}u^{(2)}(\bar{\rho}). \quad (21)$$

As for the static anomalous dimension  $\eta_\phi$ , we utilize the result with the LPA' approximation

$$\eta_\phi = \frac{8}{d} \frac{1}{2^d \pi^{d/2} \Gamma(d/2)} \frac{\bar{\rho}_0 (u^{(2)}(\bar{\rho}_0))^2}{(1 + 2\bar{\rho}_0 u^{(2)}(\bar{\rho}_0))^2}, \quad (22)$$

where  $\bar{\rho}_0$  is the minimum of the effective potential, i.e.,  $u'(\bar{\rho}_0) = 0$ .

Here we neglect the loop diagram correction for the coupling  $g_k$ . The flow for  $\bar{g}$  only comes from the running of canonical dimension. It has been proved that there is no correction for the coupling to the one-loop order in the perturbative theory [53, 54]. It has been shown that it is the combination of  $\bar{\lambda}\bar{\eta}$  that determines the scaling behavior, not the coefficients  $\bar{\lambda}$  and  $\bar{\eta}$  separately. Therefore we define a new dimensionless coupling constant

$$f = \nu_d \frac{\bar{g}^2}{\bar{\lambda}\bar{\eta}}, \quad (23)$$

with  $\nu_d = 1/[2^d \pi^{d/2} \Gamma(d/2)]$  is the geometric factor corresponding to the angular integration. By combining the flow equations of Eq. (18) to (20), one arrives at

$$\partial_\tau f = (\eta_\phi - (4 - d))f - I_\lambda f^2 - I_\eta f^2, \quad (24)$$

where the functions  $I_\lambda, I_\eta$  read

$$\begin{aligned} I_\lambda = & - \frac{2}{(1 + \bar{m}^2)^2} \int d\Omega_d (-1 + \cos^2 \theta) \cos^2 \theta \\ & + \frac{4}{d} \frac{1}{(1 + \bar{m}^2)^2} \int d\Omega_d (2 - 6\cos^2 \theta + 4\cos^4 \theta) \\ & - \frac{2}{1 + \bar{m}^2} \int d\Omega_d (\cos^4 \theta - \cos^2 \theta), \end{aligned} \quad (25)$$

$$I_\eta = \frac{2}{d} \frac{1}{(1 + \bar{m}^2)^3} \int d\Omega_d (1 - 3\cos^2 \theta + 2\cos^4 \theta). \quad (26)$$

As for the  $I_\lambda$ , the higher order terms in the Eq. (18) have been neglected. The fixed-point equation of the coupling constant  $f$  as well as its solution is readily obtained from Eq. (24).

Once we find the fixed-point solution of  $f^*$ , the anomalous dimensions of transport coefficient  $\lambda_k$  and shear viscosity  $\eta_k$  can be easily obtained according to the scaling behavior in the critical regime

$$\lambda_k \sim k^{-x_\lambda}, \quad \eta_k \sim k^{-x_\eta}, \quad (27)$$

where the exponents  $x_\lambda$  and  $x_\eta$  are the anomalous dimensions, they can be computed using the following relation:

$$x_\lambda = -I_\lambda f^*, \quad x_\eta = -I_\eta f^*. \quad (28)$$

Actually, Eq. (28) can be obtained from the right hand side of flow equations in Eq. (18) and Eq. (19). Finally, the dynamic critical exponent  $z$  of the order parameter is obtained based on Eq. (8). In the next section, we will show the numerical results of the fixed-point solution and various critical exponents.

#### IV. NUMERICAL RESULTS

In this work, the derivative of global effective potential  $u'(\bar{\rho})$  is obtained using the large field expansion method

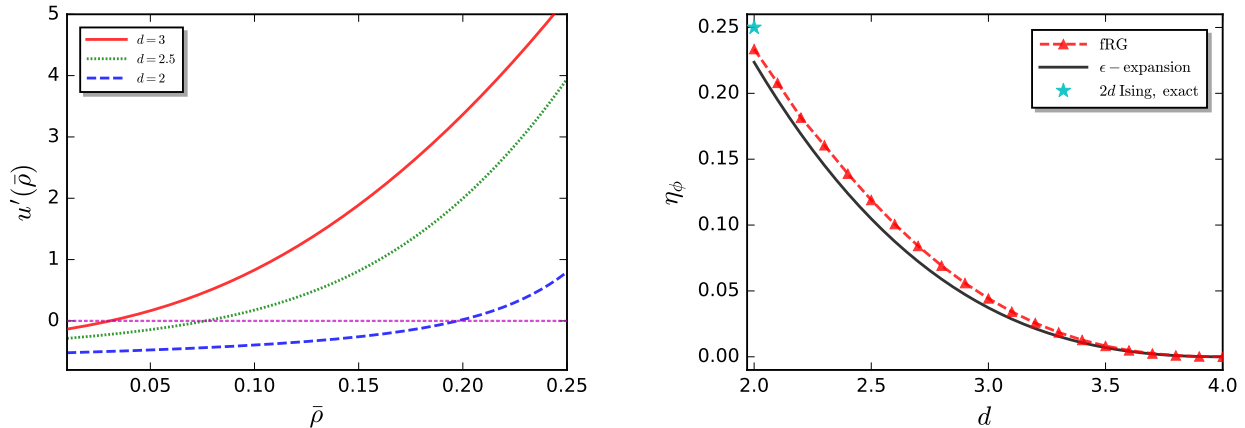


FIG. 4: Left panel: The global solution for  $u'(\bar{\rho})$  derived from the fixed-point equation Eq. (17). Right panel: The static anomalous dimension  $\eta_\phi$  as a function of spatial dimension  $d$ , including a comparison with the  $\epsilon$ -expansion result presented in Eq. (29).

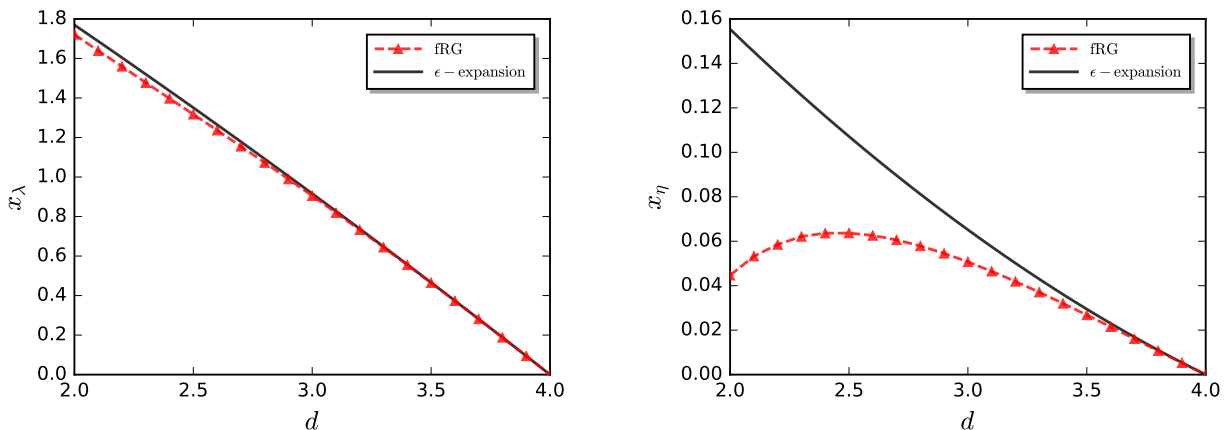


FIG. 5: The dynamic anomalous dimensions  $x_\lambda$ (left panel) and  $x_\eta$ (right panel) across various spatial dimensions  $d$ . Results from fRG calculation and  $\epsilon$ -expansion taken from [53] are summarized.

proposed in [64]. By directly solving the fixed-point equation starting from the large field asymptotic, we achieve the global effective potential with high numerical accuracy. The fixed-point value of the coupling constant  $f^*$  is then determined from the global effective potential.

In Fig. 4 we present the global solution of derivatives of the effective potential  $u'(\bar{\rho})$  as a function of  $\bar{\rho}$  for three different spatial dimensions(left panel). We also show the static anomalous dimension  $\eta_\phi$  spatial dimension  $d$  as a function of spatial dimension  $d$  which is extracted from Eq. (22)(right panel). The function  $u'(\bar{\rho})$  demonstrates monotonic behavior with respect to  $\bar{\rho}$  and possesses a unique zero, indicating the presence of the Wilson-Fisher fixed point. As the spatial dimension  $d$  decreases, the position of zero  $\bar{\rho}_0$  increases, indicating the necessity of a global solution rather than a local Taylor expansion, as discussed in [64]. In the LPA' approximation, the static

anomalous dimension follows the form given in Eq. (22), and we compare our results with the  $\epsilon$ -expansion up to the third order[65].

$$\eta = \frac{N+2}{2(N+8)^2}\epsilon^2 + \frac{N+2}{2(N+8)^2} \left[ \frac{6(3N+14)}{(N+8)^2} - \frac{1}{4} \right] \epsilon^3. \quad (29)$$

The value of  $\eta_\phi$  from fRG computation and  $\epsilon$ -expansion are comparable when  $d \geq 3.5$ . We also present the exact value  $\eta_\phi = 0.25$  for  $d = 2$  with a star in the figure.

In Fig. 5, we investigate the dependence of the dynamic anomalous dimensions  $x_\lambda, x_\eta$  on the spatial dimension  $d$ . The  $\epsilon$ -expansion results from Eq. (9) are also shown for comparison. The anomalous dimension  $x_\lambda$ , associated with the transport coefficient, shows excellent agreement with the perturbative expansion up to  $\epsilon^2$ , with deviations appearing for spatial dimensions  $d < 2.8$ . In contrast, the

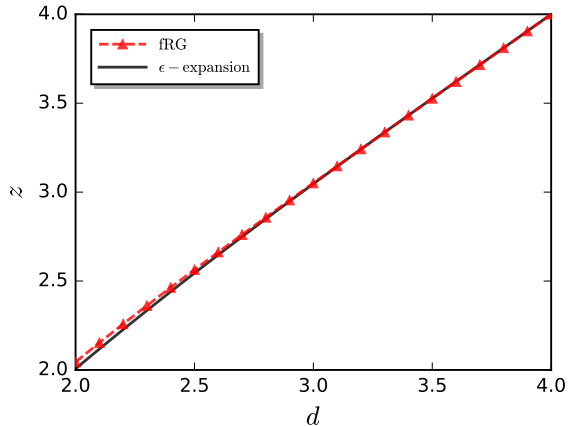


FIG. 6: Dynamical critical exponent  $z$  defined in Eq. (8) as a function of the spatial dimension  $d$ .  $\epsilon$ -expansion for  $\eta_\phi$  in Eq. (29) and  $x_\lambda$  in Eq. (9) are also presented as comparison.

behavior of  $x_\eta$  differs. Results from the fRG calculations and  $\epsilon$ -expansion are comparable only as the spatial dimension approaches 4. Additionally, our result for  $x_\eta$  exhibits non-monotonic behavior when  $d \lesssim 2.5$ .

Finally, the dynamic critical exponent  $z$  as a function of spatial dimension  $d$  is shown in Fig. 6. The anomalous dimensions  $\eta_\phi$  and  $x_\lambda$  are obtained from Fig. 4 and Fig. 5 for our real-time fRG computation, respectively. The  $\epsilon$ -expansion results for  $\eta$  are taken from Eq. (29) and for  $x_\lambda$  from Eq. (9). Since the order parameter is a conserved quantity, the dynamic critical exponent  $z = 4$  for spatial dimension  $d = 4$ . Both results are highly consistent, with only minor differences emerging as the spatial dimension approaches 2.

## V. SUMMARY AND OUTLOOK

In this work, we investigate the critical dynamics of Model H, which describes a conserved order parameter field coupled with the transverse momentum density, using the real-time fRG approach. The Langevin equation of Model H incorporates kinetic terms and coupling mode interactions. By integrating the noise terms and introducing the Martin-Siggia-Rose response field, i.e., the “q” type fields, which encode fluctuation effects in the Schwinger-Keldysh field theory, we obtain the RG scale-dependent effective action to address the dynamics with the fRG approach.

We solve the one-point and two-point correlation functions of the effective action to derive the flow equations for the effective potential, transport coefficient  $\lambda_k$ , and shear viscosity  $\eta_k$ . The contributions of mode couplings to the flow of  $\lambda_k$  and  $\eta_k$  are considered. We introduce the fixed-point equation for a coupling constant  $f$ , which determines the dynamical scaling behavior. The global

fixed-point solution of the effective potential is obtained by integrating the flow equation from large to vanishing field. Subsequently, the anomalous dimensions for the transport coefficient  $x_\lambda$  and shear viscosity  $x_\eta$  are determined according to their scaling forms in the critical regime. Finally, the dynamic critical exponent for the order parameter is computed.

Our results for the anomalous dimension  $x_\lambda$  and the dynamic critical exponent show excellent consistency with the perturbative  $\epsilon$ -expansion results from previous studies in the range  $2 \leq d \leq 4$ . Only small deviations emerge as the spatial dimension approaches 2. However, result for anomalous dimension  $x_\eta$  from fRG computation and  $\epsilon$ -expansion are comparable only in a narrow range of spatial dimensions close to 4. Additionally,  $x_\eta$  exhibits non-monotonic behavior for  $d \lesssim 2.5$ . From the previous analysis[30], the dynamics of QCD critical end point and Model H belong to the same dynamic universality class. Our results predict a dynamic critical exponent  $z = 3.0507$  for  $d = 3$ .

## ACKNOWLEDGMENTS

This work is supported by the National Natural Science Foundation of China under Grant Nos. 12175030.

### Appendix A: Propagators and mode-coupling vertices

As mentioned in Sec. III, in the real-time fRG framework, the definition of propagators correspond to two-point function of the effective action which contain the retarded, advanced and Keldysh components. The general definition of the propagator is

$$G_{\Phi_i \Phi_j, k} = \left( \frac{\delta^2 \Gamma_k[\Phi]}{\delta \Phi_i \delta \Phi_j} + R_{\Phi, k} \right)^{-1}. \quad (\text{A1})$$

Taking the functional derivative with the different types of fields in above equation. In this work, the specific forms of the propagators are

$$iG_{\phi, k}^R(q) = \frac{i}{q_0 + i\lambda_k \mathbf{q}^2 \left( \mathbf{q}^2 \left( 1 + r_B \left( \frac{\mathbf{q}^2}{k^2} \right) \right) + m_{\phi, k}^2 \right)},$$

$$iG_{\phi, k}^A(q) = \frac{i}{q_0 - i\lambda_k \mathbf{q}^2 \left( \mathbf{q}^2 \left( 1 + r_B \left( \frac{\mathbf{q}^2}{k^2} \right) \right) + m_{\phi, k}^2 \right)},$$

$$iG_{\phi, k}^K(q) = \frac{4\lambda_k \mathbf{q}^2}{q_0^2 + \left[ \lambda_k \mathbf{q}^2 \left( \mathbf{q}^2 \left( 1 + r_B \left( \frac{\mathbf{q}^2}{k^2} \right) \right) + m_{\phi, k}^2 \right) \right]^2}. \quad (\text{A2})$$

for the order parameter and

$$\begin{aligned}
iG_{j\alpha\beta,k}^R(q) &= \frac{i}{q_0 + i\eta_k \mathbf{q}^2 \left(1 + r_B\left(\frac{\mathbf{q}^2}{k^2}\right)\right)} \Pi_{\alpha\beta}^\perp, \\
iG_{j\alpha\beta,k}^A(q) &= \frac{i}{q_0 - i\eta_k \mathbf{q}^2 \left(1 + r_B\left(\frac{\mathbf{q}^2}{k^2}\right)\right)} \Pi_{\alpha\beta}^\perp, \\
iG_{j\alpha\beta,k}^K(q) &= \frac{4\eta_k \mathbf{q}^2}{q_0^2 + \left[\eta_k \mathbf{q}^2 \left(1 + r_B\left(\frac{\mathbf{q}^2}{k^2}\right)\right)\right]^2} \Pi_{\alpha\beta}^\perp. \quad (\text{A3})
\end{aligned}$$

for the transverse momentum density fields. Since the effective potential satisfy the Ising symmetry, the order parameter only has the radial component. The mass term in Eq. (A2) reads

$$m_{\phi,k}^2 = V'(\rho_c) + 2\rho_c V''(\rho_c). \quad (\text{A4})$$

The operator  $\Pi^\perp$  in Eq. (A3) selects the transverse part of vector momentum density. The regulator functions are

chosen as [66, 67]

$$R_{\phi,k}^{qc}(q) = i\lambda_k \mathbf{q}^4 r_B\left(\frac{\mathbf{q}^2}{k^2}\right), \quad R_{j,k}^{qc}(q) = i\eta_k \mathbf{q}^2 r_B\left(\frac{\mathbf{q}^2}{k^2}\right) \delta_{\mu\nu}, \quad (\text{A5})$$

where  $r_B(x)$  is a Heaviside step function  $\Theta(x)$ , that is

$$r_B(x) = \left(\frac{1}{x} - 1\right)\Theta(1-x). \quad (\text{A6})$$

For the flow equation of effective potential, the vertex  $\Gamma_{\phi_q\phi_c\phi_c,k}^{(3)}$  emerge in the right hand of Eq. (14) is

$$i\Gamma_{\phi_q\phi_c\phi_c,k}^{(3)} = -3\rho_c^{1/2} V_k^{(2)}(\rho_c) - 2\rho_c^{3/2} V_k^{(3)}(\rho_c). \quad (\text{A7})$$

To evaluate the flow equation for the two-point correlation function in Fig. 3, the higher order vertices are needed. They can be easily obtained from the functional derivative of  $\Gamma_k[\Phi]$  w.r.t the corresponding fields  $\phi$ (or  $j$ ). In this work, the three-point vertices contribute from the coupling modes read

$$i\Gamma_{\phi_q\phi_c j_c,k}^{(3)}(q_1, q_2, q_3) = g_k \mathbf{q}_2 \cdot \mathbf{e}_{j_c}, \quad (\text{A8})$$

$$i\Gamma_{j_q\phi_c\phi_c,k}^{(3)}(q_1, q_2, q_3) = -g_k \mathbf{q}_3^2 \mathbf{e}_{j_q} \cdot \mathbf{q}_2 - g_k \mathbf{q}_2^2 \mathbf{e}_{j_q} \cdot \mathbf{q}_3, \quad (\text{A9})$$

where the explicit momentum dependence from the "classical" fields are labelled. And the  $\mathbf{e}_j$  is the unit vector along the  $\mathbf{j}$  field direction.

## Appendix B: Loop diagram calculation

In this appendix, we give a specific example to show how the calculation are performed and what approximation are made. We employ a loop diagram for the two-point correlation function  $\Gamma_{\phi_q\phi_c,k}^{(2)}$  with the regulator function inserting on the order parameter propagator, that is,

$$\begin{aligned}
\text{---} \overset{q}{\circlearrowleft} \text{---} &= \int_q \partial_\tau R_{\phi,k} G_{\phi,k}^A(q) \Gamma_{\phi_q\phi_c j_c,k}^{(3)} G_{j,k}^K(q-p) \Gamma_{\phi_q\phi_c j_c,k}^{(3)} G_{\phi,k}^A(q). \quad (\text{B1})
\end{aligned}$$

Taking the expression of vertices and propagators in App. A into the above equation, one has

$$\begin{aligned}
&\int_q \partial_\tau R_{\phi,k} \frac{1}{\left[ i q_0 + \lambda_k \mathbf{q}^2 \left( \mathbf{q}^2 \left( 1 + r_B\left(\frac{\mathbf{q}^2}{k^2}\right) \right) + m_{\phi,k}^2 \right) \right]^2} \times \frac{4\eta_k (\mathbf{q}-\mathbf{p})^2}{(q_0-p_0)^2 + \left[ \eta_k (\mathbf{q}-\mathbf{p})^2 \left( 1 + r_B\left(\frac{(\mathbf{q}-\mathbf{p})^2}{k^2}\right) \right) \right]^2} \\
&\quad g_k(i\mathbf{q}_\mu) \times \left( \delta^{\mu\nu} - \frac{(\mathbf{q}-\mathbf{p})_\mu (\mathbf{q}-\mathbf{p})_\nu}{(\mathbf{q}-\mathbf{p})^2} \right) \times g_k(-i\mathbf{p}_\nu) \\
&= \int_q \partial_\tau R_{\phi,k} g_k^2 (-1 + \cos^2 \theta) \mathbf{q}^2 \mathbf{p}^2 \frac{4\eta_k}{q_0^2 + \left[ \eta_k \mathbf{q}^2 \left( 1 + r_B\left(\frac{\mathbf{q}^2}{k^2}\right) \right) \right]^2} \frac{1}{\left[ i q_0 + \lambda_k \mathbf{q}^2 \left( \mathbf{q}^2 \left( 1 + r_B\left(\frac{\mathbf{q}^2}{k^2}\right) \right) + m_{\phi,k}^2 \right) \right]^2} \quad (\text{B2})
\end{aligned}$$

The vertices keep the external momentum to order 2. Since the flow equation for transport coefficient  $\lambda_k$  project onto the  $p^4$  term, we need to expand the  $G_{j,k}^K$  propagator about the external momentum. The result is given by

$$-\frac{1}{2} \frac{1}{[q_0^2/k^2 + (\eta_k x(1+r_B(x)))^2]^2} 2\eta_k^2 \delta(1-x) \frac{4(\mathbf{q} \cdot \mathbf{p})^2}{k^4} \quad (\text{B3})$$

where  $x = \mathbf{q}^2/k^2$  is the ratio of internal momentum over RG scale.

Now we complete the integration in Eq. (B2),

$$\frac{1}{(2\pi)^d} \int d\mathbf{x} d\Omega_D k^d x^{\frac{d}{2}} 16g_k^2 \lambda_k \eta_k^3 (-1 + \cos^2 \theta) \cos^2 \theta \mathbf{q}^4 \mathbf{p}^4 \frac{1}{k^{16}} \frac{k^6(3\eta_k + \lambda_k k^2 x(1 + \bar{m}^2))}{4\eta_k^3(\eta_k + \lambda_k k^2 x(1 + \bar{m}^2))^3} \delta(1-x) \quad (\text{B4})$$

Here comes to the most important approximation we made in order to get the final result, the shear viscosity  $\eta_k$  grows large with the running of RG scale while  $\lambda_k$  approaches to a finite value in the IR. With the RG scale evolving to IR, we have  $\eta_k \gg \lambda_k$ . So the  $\lambda_k k^2$  term in the denominator can be neglected and we get the final expression

$$\frac{1}{(2\pi)^d} \int d\Omega_D \frac{6\bar{g}^2}{\bar{\eta}^2} (-1 + \cos^2 \theta) \cos^2 \theta \lambda_k \mathbf{p}^4 \quad (\text{B5})$$

- 
- [1] C. S. Fischer, QCD at finite temperature and chemical potential from Dyson-Schwinger equations, *Prog. Part. Nucl. Phys.* **105**, 1 (2019), [arXiv:1810.12938 \[hep-ph\]](#).
- [2] N. Dupuis, L. Canet, A. Eichhorn, W. Metzner, J. M. Pawłowski, M. Tissier, and N. Wschebor, The nonperturbative functional renormalization group and its applications, *Phys. Rept.* **910**, 1 (2021), [arXiv:2006.04853 \[cond-mat.stat-mech\]](#).
- [3] W.-j. Fu, QCD at finite temperature and density within the fRG approach: an overview, *Commun. Theor. Phys.* **74**, 097304 (2022), [arXiv:2205.00468 \[hep-ph\]](#).
- [4] J. Braun *et al.*, Soft modes in hot QCD matter, (2023), [arXiv:2310.19853 \[hep-ph\]](#).
- [5] M. Bluhm *et al.*, Dynamics of critical fluctuations: Theory – phenomenology – heavy-ion collisions, *Nucl. Phys. A* **1003**, 122016 (2020), [arXiv:2001.08831 \[nucl-th\]](#).
- [6] X. Luo and N. Xu, Search for the QCD Critical Point with Fluctuations of Conserved Quantities in Relativistic Heavy-Ion Collisions at RHIC : An Overview, *Nucl. Sci. Tech.* **28**, 112 (2017), [arXiv:1701.02105 \[nucl-ex\]](#).
- [7] M. Stephanov, Non-Gaussian fluctuations near the QCD critical point, *Phys. Rev. Lett.* **102**, 032301 (2009), [arXiv:0809.3450 \[hep-ph\]](#).
- [8] W.-j. Fu, X. Luo, J. M. Pawłowski, F. Rennecke, R. Wen, and S. Yin, Hyper-order baryon number fluctuations at finite temperature and density, *Phys. Rev. D* **104**, 094047 (2021), [arXiv:2101.06035 \[hep-ph\]](#).
- [9] W.-j. Fu, X. Luo, J. M. Pawłowski, F. Rennecke, and S. Yin, Ripples of the QCD Critical Point, (2023), [arXiv:2308.15508 \[hep-ph\]](#).
- [10] L. Adamczyk *et al.* (STAR), Energy Dependence of Moments of Net-proton Multiplicity Distributions at RHIC, *Phys. Rev. Lett.* **112**, 032302 (2014), [arXiv:1309.5681 \[nucl-ex\]](#).
- [11] L. Adamczyk *et al.* (STAR), Bulk Properties of the Medium Produced in Relativistic Heavy-Ion Collisions from the Beam Energy Scan Program, *Phys. Rev. C* **96**, 044904 (2017), [arXiv:1701.07065 \[nucl-ex\]](#).
- [12] A. Bzdak, S. Esumi, V. Koch, J. Liao, M. Stephanov, and N. Xu, Mapping the Phases of Quantum Chromodynamics with Beam Energy Scan, *Phys. Rept.* **853**, 1 (2020), [arXiv:1906.00936 \[nucl-th\]](#).
- [13] J. Adam *et al.* (STAR), Nonmonotonic Energy Dependence of Net-Proton Number Fluctuations, *Phys. Rev. Lett.* **126**, 092301 (2021), [arXiv:2001.02852 \[nucl-ex\]](#).
- [14] W.-j. Fu, J. M. Pawłowski, and F. Rennecke, QCD phase structure at finite temperature and density, *Phys. Rev. D* **101**, 054032 (2020), [arXiv:1909.02991 \[hep-ph\]](#).
- [15] F. Gao and J. M. Pawłowski, Chiral phase structure and critical end point in QCD, *Phys. Lett. B* **820**, 136584 (2021), [arXiv:2010.13705 \[hep-ph\]](#).
- [16] P. J. Gunkel and C. S. Fischer, Locating the critical endpoint of QCD: Mesonic backcoupling effects, *Phys. Rev. D* **104**, 054022 (2021), [arXiv:2106.08356 \[hep-ph\]](#).
- [17] A. Sorensen and P. Sorensen, Locating the critical point for the hadron to quark-gluon plasma phase transition from finite-size scaling of proton cumulants in heavy-ion collisions, (2024), [arXiv:2405.10278 \[nucl-th\]](#).
- [18] D. A. Clarke, P. Dimopoulos, F. Di Renzo, J. Goswami, C. Schmidt, S. Singh, and K. Zambello, Searching for the QCD critical endpoint using multi-point Padé approximations, (2024), [arXiv:2405.10196 \[hep-lat\]](#).
- [19] R. D. Pisarski and F. Wilczek, Remarks on the Chiral Phase Transition in Chromodynamics, *Phys. Rev. D* **29**, 338 (1984).
- [20] A. M. Halasz, A. D. Jackson, R. E. Shrock, M. A. Stephanov, and J. J. M. Verbaarschot, On the phase diagram of QCD, *Phys. Rev. D* **58**, 096007 (1998), [arXiv:hep-ph/9804290](#).
- [21] Y.-r. Chen, R. Wen, and W.-j. Fu, Critical behaviors of the O(4) and Z(2) symmetries in the QCD phase diagram, *Phys. Rev. D* **104**, 054009 (2021), [arXiv:2101.08484 \[hep-ph\]](#).
- [22] K. Rajagopal and F. Wilczek, Static and dynamic criti-



- cal phenomena at a second order QCD phase transition, *Nucl. Phys. B* **399**, 395 (1993), [arXiv:hep-ph/9210253](#).
- [23] B. Berdnikov and K. Rajagopal, Slowing out-of-equilibrium near the QCD critical point, *Phys. Rev. D* **61**, 105017 (2000), [arXiv:hep-ph/9912274](#).
- [24] B. I. Halperin, P. C. Hohenberg, and S.-k. Ma, Calculation of Dynamic Critical Properties Using Wilson's Expansion Methods, *Phys. Rev. Lett.* **29**, 1548 (1972).
- [25] B. I. Halperin, P. C. Hohenberg, and S.-k. Ma, Renormalization-group methods for critical dynamics: 1. Recursion relations and effects of energy conservation, *Phys. Rev. B* **10**, 139 (1974).
- [26] B. I. Halperin, P. C. Hohenberg, and S.-k. Ma, Renormalization-group methods for critical dynamics: 2. Detailed analysis of the relaxational models, *Phys. Rev. B* **13**, 4119 (1976).
- [27] B. I. Halperin, P. C. Hohenberg, and E. D. Siggia, Renormalization-group treatment of the critical dynamics of superfluid helium, the isotropic antiferromagnet, and the easy-plane ferromagnet, *Phys. Rev. B* **13**, 1299 (1976).
- [28] P. C. Hohenberg and B. I. Halperin, Theory of Dynamic Critical Phenomena, *Rev. Mod. Phys.* **49**, 435 (1977).
- [29] R. Folk and G. Moser, Critical dynamics: a field-theoretical approach, *Journal of Physics A: Mathematical and General* **39**, R207 (2006).
- [30] D. T. Son and M. A. Stephanov, Dynamic universality class of the QCD critical point, *Phys. Rev. D* **70**, 056001 (2004), [arXiv:hep-ph/0401052](#).
- [31] J. Berges, S. Schlichting, and D. Sexty, Dynamic critical phenomena from spectral functions on the lattice, *Nucl. Phys. B* **832**, 228 (2010), [arXiv:0912.3135 \[hep-lat\]](#).
- [32] S. Schlichting, D. Smith, and L. von Smekal, Spectral functions and critical dynamics of the  $O(4)$  model from classical-statistical lattice simulations, *Nucl. Phys. B* **950**, 114868 (2020), [arXiv:1908.00912 \[hep-lat\]](#).
- [33] D. Schweitzer, S. Schlichting, and L. von Smekal, Spectral functions and dynamic critical behavior of relativistic  $Z_2$  theories, *Nucl. Phys. B* **960**, 115165 (2020), [arXiv:2007.03374 \[hep-lat\]](#).
- [34] D. Schweitzer, S. Schlichting, and L. von Smekal, Critical dynamics of relativistic diffusion, *Nucl. Phys. B* **984**, 115944 (2022), [arXiv:2110.01696 \[hep-lat\]](#).
- [35] A. Florio, E. Grossi, A. Soloviev, and D. Teaney, Dynamics of the  $O(4)$  critical point in QCD, *Phys. Rev. D* **105**, 054512 (2022), [arXiv:2111.03640 \[hep-lat\]](#).
- [36] A. Florio, E. Grossi, and D. Teaney, Dynamics of the  $O(4)$  critical point in QCD: critical pions and diffusion in Model G, (2023), [arXiv:2306.06887 \[hep-lat\]](#).
- [37] J. Berges and G. Hoffmeister, Nonthermal fixed points and the functional renormalization group, *Nucl. Phys. B* **813**, 383 (2009), [arXiv:0809.5208 \[hep-th\]](#).
- [38] T. Gasenzer and J. M. Pawłowski, Towards far-from-equilibrium quantum field dynamics: A functional renormalisation-group approach, *Phys. Lett. B* **670**, 135 (2008), [arXiv:0710.4627 \[cond-mat.other\]](#).
- [39] J. M. Pawłowski and N. Strodthoff, Real time correlation functions and the functional renormalization group, *Phys. Rev. D* **92**, 094009 (2015), [arXiv:1508.01160 \[hep-ph\]](#).
- [40] L. Corell, A. K. Cyrol, M. Heller, and J. M. Pawłowski, Flowing with the temporal renormalization group, *Phys. Rev. D* **104**, 025005 (2021), [arXiv:1910.09369 \[hep-th\]](#).
- [41] J. Braun *et al.*, Renormalised spectral flows, *SciPost Phys. Core* **6**, 061 (2023), [arXiv:2206.10232 \[hep-th\]](#).
- [42] S. Huelsmann, S. Schlichting, and P. Scior, Spectral functions from the real-time functional renormalization group, *Phys. Rev. D* **102**, 096004 (2020), [arXiv:2009.04194 \[hep-ph\]](#).
- [43] Y.-y. Tan, Y.-r. Chen, and W.-j. Fu, Real-time dynamics of the  $O(4)$  scalar theory within the fRG approach, *SciPost Phys.* **12**, 026 (2022), [arXiv:2107.06482 \[hep-ph\]](#).
- [44] J. V. Roth, D. Schweitzer, L. J. Sieke, and L. von Smekal, Real-time methods for spectral functions, *Phys. Rev. D* **105**, 116017 (2022), [arXiv:2112.12568 \[hep-ph\]](#).
- [45] Y.-y. Tan, Y.-r. Chen, W.-j. Fu, and W.-J. Li, Universality of pseudo-Goldstone damping near critical points, (2024), [arXiv:2403.03503 \[hep-th\]](#).
- [46] J. V. Roth and L. von Smekal, Critical dynamics in a real-time formulation of the functional renormalization group, *JHEP* **10**, 065, [arXiv:2303.11817 \[hep-ph\]](#).
- [47] Y.-r. Chen, Y.-y. Tan, and W.-j. Fu, Critical dynamics within the real-time FRG approach, *Phys. Rev. D* **109**, 094044 (2024), [arXiv:2312.05870 \[hep-ph\]](#).
- [48] L. Canet and H. Chaté, A non-perturbative approach to critical dynamics, *Journal of Physics A: Mathematical and Theoretical* **40**, 1937 (2007), [arXiv:cond-mat/0610468](#).
- [49] L. Canet, H. Chate, and B. Delamotte, General framework of the non-perturbative renormalization group for non-equilibrium steady states, *J. Phys. A* **44**, 495001 (2011), [arXiv:1106.4129 \[cond-mat.stat-mech\]](#).
- [50] L. Batini, E. Grossi, and N. Wink, Dissipation dynamics of a scalar field, *Phys. Rev. D* **108**, 125021 (2023), [arXiv:2309.06586 \[hep-th\]](#).
- [51] D. Mesterházy, J. H. Stockemer, L. F. Palhares, and J. Berges, Dynamic universality class of Model C from the functional renormalization group, *Phys. Rev. B* **88**, 174301 (2013), [arXiv:1307.1700 \[cond-mat.stat-mech\]](#).
- [52] J. V. Roth, Y. Ye, S. Schlichting, and L. von Smekal, Dynamic critical behavior of the chiral phase transition from the real-time functional renormalization group, (2024), [arXiv:2403.04573 \[hep-ph\]](#).
- [53] E. D. Siggia, B. I. Halperin, and P. C. Hohenberg, Renormalization-group treatment of the critical dynamics of the binary-fluid and gas-liquid transitions, *Phys. Rev. B* **13**, 2110 (1976).
- [54] H.-U. Yee, Dynamic universality class of model H with frustrated diffusion:  $\epsilon$  expansion, *Phys. Rev. D* **97**, 016003 (2018), [arXiv:1707.08560 \[hep-ph\]](#).
- [55] C. Chattopadhyay, J. Ott, T. Schaefer, and V. V. Skokov, Simulations of stochastic fluid dynamics near a critical point in the phase diagram, (2024), [arXiv:2403.10608 \[nucl-th\]](#).
- [56] J. S. Schwinger, Brownian motion of a quantum oscillator, *J. Math. Phys.* **2**, 407 (1961).
- [57] L. V. Keldysh, Diagram technique for nonequilibrium processes, *Zh. Eksp. Teor. Fiz.* **47**, 1515 (1964).
- [58] B. I. Halperin and P. C. Hohenberg, Scaling Laws for Dynamic Critical Phenomena, *Phys. Rev.* **177**, 952 (1969).
- [59] G. Arcovito, C. Faloci, M. Roberti, and L. Mistura, Shear viscosity of the binary system aniline-cyclohexane near the critical point, *Phys. Rev. Lett.* **22**, 1040 (1969).
- [60] S.-M. Lo and K. Kawasaki, Frequency-dependence correction to the order-parameter decay rates near the critical point of fluids, *Phys. Rev. A* **8**, 2176 (1973).
- [61] C. Wetterich, Exact evolution equation for the effective potential, *Phys. Lett. B* **301**, 90 (1993), [arXiv:1710.05815](#)

- [62] J. M. Pawłowski, Aspects of the functional renormalisation group, *Annals Phys.* **322**, 2831 (2007), [arXiv:hep-th/0512261 \[hep-th\]](#).
- [63] P. C. Martin, E. D. Siggia, and H. A. Rose, Statistical Dynamics of Classical Systems, *Phys. Rev. A* **8**, 423 (1973).
- [64] Y.-y. Tan, C. Huang, Y.-r. Chen, and W.-j. Fu, Criticality of the  $O(N)$  universality via global solutions to nonperturbative fixed-point equations, (2022), [arXiv:2211.10249 \[hep-ph\]](#).
- [65] K. G. Wilson, Feynman graph expansion for critical exponents, *Phys. Rev. Lett.* **28**, 548 (1972).
- [66] D. F. Litim, Optimization of the exact renormalization group, *Phys. Lett.* **B486**, 92 (2000), [arXiv:hep-th/0005245 \[hep-th\]](#).
- [67] D. F. Litim, Optimized renormalization group flows, *Phys. Rev.* **D64**, 105007 (2001), [arXiv:hep-th/0103195 \[hep-th\]](#).